# Physic-based vs data-based digital twins for bush bearing wear diagnostic

Amandine Regis, Santiago Arroyave-Tobón, Jean-Marc Linares, Emmanuel Mermoz

# Physic-based vs data-based digital twins for bush bearing wear diagnostic

**Authors**

- Amandine Regis[a,b*]
- Santiago Arroyave-Tobon[a]
- Jean-Marc Linares[a]
- Emmanuel Mermoz[a,b]

a. Aix Marseille Univ, CNRS, ISM, Marseille, France
b. Airbus Helicopters, Aéroport International Marseille Provence, 13725 Marignane CEDEX, France
* Corresponding author, e-mail address: amandine.regis@univ-amu.fr

**Abstract**

Industry is increasingly turning to predictive maintenance by using digital twins (DTs) to follow and predict evolution of mechanical system. This article presents, compares and discusses two DTs to diagnose wear of bush bearings under dynamic loads. The first DT is driven by a model based on data analysis using statistical process control (SPC). The second DT is based on physical laws: Boussinesq's and Archard's equations. Both DTs are fed by data recorded on a test bench instrumented with sensors of temperature, acceleration and displacement. Rules for fault detection were identified, explained and applied to the two DTs implemented. The two implemented DTs detected abnormal wear behaviours. The data-based DT using the SPC is easier to implement and it detects change in wear behaviour earlier. In contrast, the physic-based DT has the advantage of being predictive, so it can be used when only the operating conditions of the system are known. This work is a contribution for new wear diagnostic tools.

**Keywords**

Wear
Bush bearing
Digital twin
Diagnostic tool

**Highlights**

- Implementation of a digital twin to monitor wear of a bush bearing system.
- Wear monitored through statistical process control and specific numerical model.
- Comparison of digital twin architecture.
- Design and use of a test bench instrumented with sensors.

## 1. Introduction

Wear is a critical phenomenon in dynamic systems of helicopters. Currently, wear monitoring is done by preventive maintenance at regular intervals. However, this type of maintenance is expensive [1]. Nowadays, industries are increasingly turning to predictive maintenance by using, for example, digital twins (DTs).

A DT is a virtual replica of a physical system and both exchange data and information throughout the whole life cycle of the physical system [2]. The DT perceives its environment through sensors [3] and the data flow between the virtual replica and the physical system can be either unidirectional or bidirectional [4].

In mechanical engineering, DTs have the advantage reducing maintenance costs because they allow to mirror systems where direct inspection is not easy [1]. In consequence, it allows increasing safety by detecting problems earlier [5,6]. They can be used to facilitate the lifecycle management [5,7], to support manufacturing processes [8–10] and to monitor or predict mechanical damages [11–16].

DTs are supported by models based on data analysis or on physical laws.

Data-based models are created from the analysis of data recorded by the studied system sensors. The analysis of recorded data can be done through different approaches. Neural network and machine learning have been used to analyse the degradation performance of rolling bearing and to predict the remaining useful life of rolling bearing [14,16]. In [13], the authors predicted the wear of a circular blade from historic data collected with a SCADA system. In [17], a probabilistic Gaussian mixture model is used to develop a specific strategy for bearing fault detection.

Physic-based models use physical laws to describe the behaviour of the system studied. One way to implement physic-based models is by means of the finite element method (FEM). In [15], the authors used FEM in a DT to simulate automotive brake pad wear. FEM with mesh updating was used to predict fretting wear of spline couplings [18] and to predict wear on classic bush bearings [19] and bio-inspired bush bearings [20]. Specific numerical models are another way to develop physic-based model. Specific numerical models have been developed to predict wear of bearings under dynamic loads [21], revolute joint in 4-bar mechanisms [22,23], gears [24] and crossed steel wires [25]. Specific numerical models have the advantage of being less time consuming than FEM [21,22]. However, in the case of wear monitoring, FEM is well adapted to complex contact geometries.

In this work, two DTs (a data-based and a physic-based) are developed, implemented and compared. This with aim of monitoring wear of a bush bearing system mounted on a test bench. The first DT relies on a data-based model using the statistical process control (SPC). The SPC allows to continuously monitor the evolution of wear rate of the bearings. The second DT uses the specific numerical model developed by [21]. Rules of fault detection were defined to monitor a variable with linear evolution such as wear. These rules were applied on both DTs implemented.

The objective of this article is to monitor wear of a bush bearing system by means of DTs. Two DTs are implemented and compared in terms of implementation time, execution time and detection capability. This with the aim of identifying the advantages of each type of DT in the case of wear monitoring.

## 2. Material and Methods

The global architecture of both bush bearing DTs implemented in this work is presented in Fig. 1. This architecture can be divided into four components.

The first component (green box in in Fig. 1) is the physical system. In this work, it is a test bench of a bush bearing instrumented with temperature, acceleration and displacement sensors to monitor wear effects.

The second component (black box in in Fig. 1) corresponds to the transmission of data collected on the physical system to the DTs model. Data collected by the optical displacement sensor was used to identify the operating configuration (rotational speed and force loading) and to monitor wear effects over time. The other sensors were employed to control the stability of the temperature and vibrations during experiments.

The third component (blue box in in Fig. 1) is the DT to follow wear of the bush bearings. Two models were implemented in this work: one model based on data analysis using Statistical Process Control (SPC) and one model based on physic laws using a specific numerical model [21].

The last component (red box in in Fig. 1) apply the rules of fault detection.

In this section, each component of the architecture of the DTs is detailed.

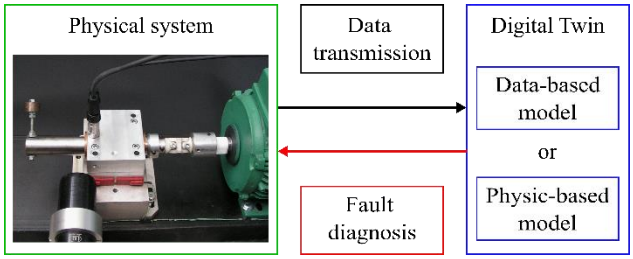


**Fig. 1.** Global architecture of DTs implemented.

### 2.1. Physical system

#### 2.1.1. Experimental test bench

The test bench of the bush bearing system is illustrated in Fig. 2. It is composed of a steel shaft OTMT 81001300 (item n°6 in Fig. 2) guided by two bronze bearings SINT A50 (item n°7 in Fig. 2). The

material properties of the shaft and the bearings are summarized in Table 1. For the tests considered in this work, no lubrication was used, only dry contact to consider the worst operating case. The initial clearance on diameter between the shaft and the bearings was 0.144 mm. An unbalanced mass (50 or 75 g) fixed at the end of the shaft (item n°1 in Fig. 2) was used to create a dynamic load. A double universal joint was used (item n°4 in Fig. 2) to connect the shaft to the motor (item n°5 in Fig. 2) and reduce parasitic dynamic loads due to misalignment between the shaft and the electric motor shaft. The frame (item n°3 in Fig. 2) of the test bench was made of aluminium alloy to diffuse the temperature generated by the friction. Before each trial, the test bench was heated to the operating temperature (38-40°C) by using an external heat source. The rotational speed was constant and equal to 1000 rpm. The two unbalanced masses were alternatively used during tests. Table 2 presents the details about the operating conditions (OC) through time.

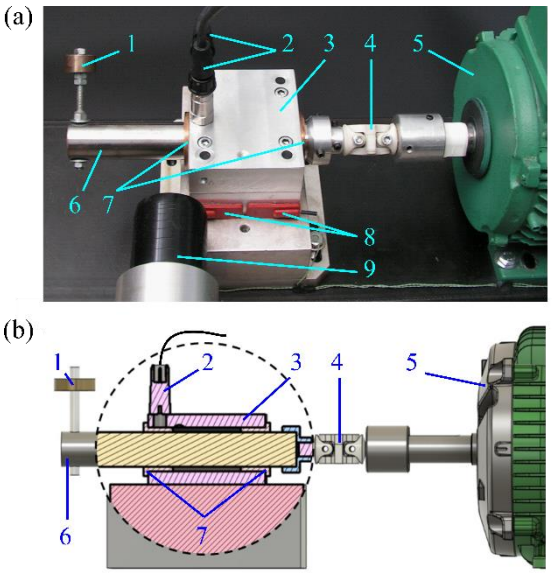


**Fig. 2.** Experimental test bench: (a) test bench photo; (b) test bench. (1) unbalanced mass; (2) accelerometers; (3) frame; (4) double universal joint; (5) motor; (6) shaft; (7) bearings; (8) thermal sensors; (9) displacement sensor.

| | Shaft | Bearing |
|---|---|---|
| Material | Steel 115Cr2 | Bronze CuSn10 |
| Young's modulus | 206 GPa | 65 GPa |
| Roughness ($R_a$) | 0.3 – 0.6 | 0.3 |
| Hardness | 54 – 56 HRC | 25 HB |

**Table 1**. Material properties of the shaft and the bearings.

| | OC 1 | OC 2 | OC 3 | OC 4 |
|---|---|---|---|---|
| Start time | 0h | 5h30 | 8h20 | 10h |
| End time | 5h30 | 8h20 | 10h | 13h |
| Unbalanced mass | 50 g | 75 g | 50 g | 75 g |

**Table 2**. Operating conditions (OC) of the experiments.

The test bench was instrumented with several sensors. Two temperature sensors (IEC type K silicone rubber patch thermocouple) were fixed on the frame (item n°8 in Fig. 2). Two accelerometers (Model 603C01 - PCB Piezotronics) were used to monitor the stability of the experiment (item n°2 in Fig. 2): one was positioned to detect vertical vibrations and the other for horizontal vibrations. A confocal chromatic displacement sensor (Micro-Epsilon IFS2405-10) was mounted perpendicular to the shaft axis to measure its displacement (run-out) (item n°9 in Fig. 2). During the experiments, data was collected every 10 minutes for 2 seconds with a NI data acquisition card. The acquisition frequencies and the monitored parameters are presented in Table 3.

| | Frequency | Monitored parameters |
|---|---|---|
| Thermal sensor | 50 Hz | Mean value of the recorded signal |
| Accelerometer | 1000 Hz | Amplitude of the recorded signal |
| Displacement sensor | 1000 Hz | Mean of the peak-to-peak of the recorded signal |

**Table 3**. Acquisition parameters of the used sensors.

In addition, the wear depth of the shaft and the bearings was measured after disassembly. To allow the disassembly of the bearings, the frame was designed in two parts and assembled using 4 screws (ISO screw M6). The screws were tightened each time they were assembled using a torque wrench in order to guarantee an identical tightening torque at each reassembly. The tightening torque was set to 5 Nm. Fig. 3 illustrates the worn shaft and bearings. For the shaft, the mean wear depth was obtained by measuring profiles of 50 mm long on the wear zones (blue line in Fig. 3a) with a micromesure station (STIL Marposs, Micromesure 2). For the bearings, the inner surface was acquired with a coordinate-measuring machine (Messwelk, MM 1004 E Trimesures). One circular path at each end of the bearings was measured (blue lines in Fig. 3b). Each circular path was composed of 36 points uniformly distributed. The wear depth of the bearing was assumed to be the diameter variation between the initial and the final circular paths.

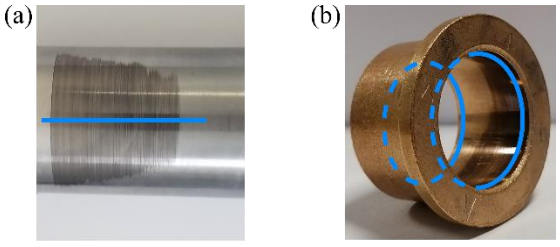


**Fig. 3.** Picture of (a) worn shaft and (b) worn bearing with the measurement paths.

### 2.1.2. Identification of operating configurations

In this work, it is assumed that the loading to which the system is subjected is not known during the operation of the system.

In order to launch the digital twin, the operating conditions of the monitored system are automatically identified from experimental data. The general workflow of this procedure is represented in Fig. 4a. The features of the shaft displacement signal (Fig. 4b) and its Fast Fourier Transformation (FFT) (Fig. 4c) were used to do so. The loading was deduced from the amplitude of the first peak of the FFT of the signal. The signal processing toolbox of Matlab, and more precisely, the classification learner tool was used. A feed forward network with a single internal layer was trained with sets of data where the unbalanced mass was known.

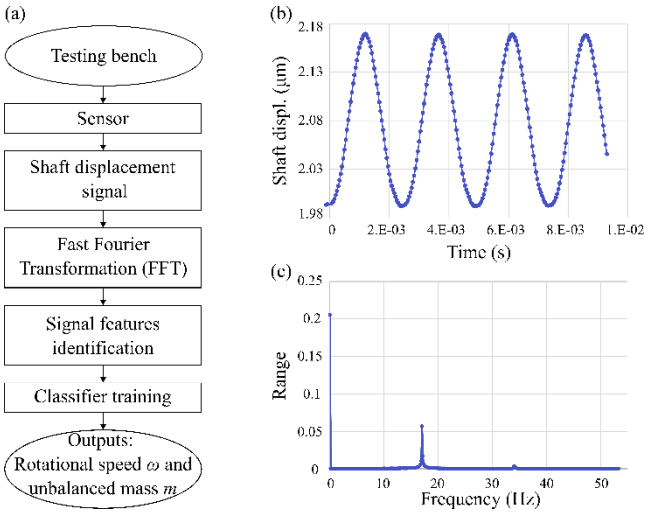


**Fig. 4.** Detection of the operating configurations using neural network of Matlab: (a) flow chart used to identify operating configurations; (b) shaft displacement signal; (c) Fast Fourier Transformation (FFT) of the shaft displacement signal.

## 2.2. Digital twins

In this section, the implementation of the DTs to diagnose wear of bush bearings under dynamic loads is described. DT models can be based on data or on physic laws. This article presents one example of each model. The data-based model was developed using SPC of the data recorded by the sensors. The physic-based model corresponds to a specific numerical model that predict the wear evolution of bearing under dynamic loading. All results presented in this article are for the stable wear stage.

### 2.2.1. Controlled variables

The aim of the DTs developed in this work is to control wear through time. The controlled variables are the wear depth and the wear rate. The wear depth is deduced from the peak-to-peak value of the shaft displacement signal (Fig. 5). From the displacement sensor measure $d_1$ and by geometric relations, the displacement $d_0$ at the end of the bearing can be calculated. This distance $d_0$ corresponds to the sum of the wear depths of the two bearings and the clearance on the diameter. The wear depth equation is defined in Fig. 5. The wear rate is defined as the wear depth per time unit (µm/h).

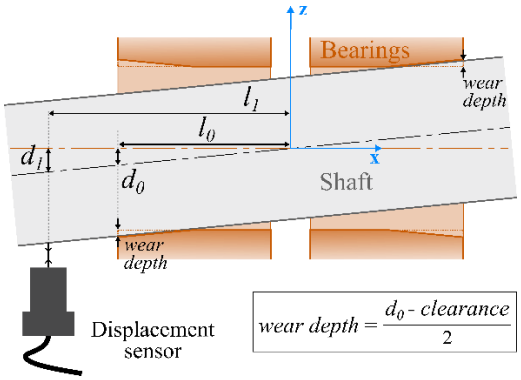


**Fig. 5.** Wear depth from displacement sensor measurement.

### 2.2.2. Data-based model

SPC was used to control the mean and the standard deviation of the wear rate to study its trend and variation. Both, the mean and the standard deviation of the wear rate, were deduced from the measured displacements. As this work is focused on the stable wear stage, the wear depth is supposed to evolve linearly through time. A linear regression of the wear depth through the time was done to determine the mean wear rate which corresponds to the slope of the regression. This regression was carried out using both the least squares and the Moore-Penrose inverse methods [26,27]. This allowed to determine the mean and the standard deviation of the wear rate.

The data controlled were supposed to follow normal distribution. The upper control limit (UCL) and the lower control limit (LCL) for the mean wear rate, respectively $UCL_\mu$ and $LCL_\mu$, and the upper control limit of the standard deviation of the wear rate, $UCL_\sigma$, are calculated as follows [28]:

$$UCL_\mu = \mu + \frac{t\,\sigma}{\sqrt{n}} \quad (1)$$

$$LCL_\mu = \mu - \frac{t\,\sigma}{\sqrt{n}} \quad (2)$$

$$UCL_\sigma = B_4\,\sigma \quad (3)$$

where $n$ is the size of the sample, $\mu$ the mean wear rate target (see Table 4 for numerical values), $\sigma$ the standard deviation target of the wear rate (see Table 4 for numerical values), $t$ the coverage factor determined by the inverse of Student's law with a risk of 0.25% and $B_4$ the coefficient for the calculation of the control limit from [28]. The mean target $\mu$ and the standard deviation target $\sigma$ were obtained from calibration tests.

| | $\mu$ (µm/h) | $\sigma$ (µm/h) |
|---|---|---|
| $m$ = 50 g | 0.933 | 0.320 |
| $m$ = 75 g | 1.412 | 0.389 |

**Table 4.** Target values for the mean and the standard deviation of the wear rate for unbalanced mass of 50 g and 75 g.

### 2.2.3. Physic-based model

The numerical model to predict wear of bush bearings under off-centred dynamic loads is summarized hereafter. The algorithm behind this model is presented in Fig. 6. For more details readers can refer to [21].

**Algorithm**: Numerical Wear Model

**Inputs**: unbalanced mass $m$;
rotational speed $\omega$;
initial time $t_0$;
pressure distribution equation $P(x,z)$;
wear distribution equation $h(x,z)$;
wear coefficient $K$.
**Output**: wear depth in function of time.

1. Compute bearing reaction forces from the force balance;
2. **while** $t_i < t_{end}$ , ***do***
3. Compute the contact pressure and contact area from the Boussinesq's equation;
4. Compute the wear volume from the Archard's law;
5. Compute the wear depth;
6. Compute the cumulative wear;
7. $t_i = t_{i+1}$ and geometry update;
8. **end while**

**Fig. 6.** Pseudo algorithm of the wear numerical model.

Several input parameters are necessary to run the model. The time is initialized to $t_0$. The rotational speed of the shaft $\omega$, the unbalanced mass $m$ and the wear coefficients $K$ are required. The contact pressure distribution field $P(x,z)$ and the wear distribution field $h(x,z)$ are supposed to be sinusoidal [29] in the plane with normal **x** (Fig. 7a) and linear in the plane with normal **z** (Fig. 7b). The boundary of the fields on the shaft corresponds to the contact area and is assumed to be parabolic (Fig. 7c).

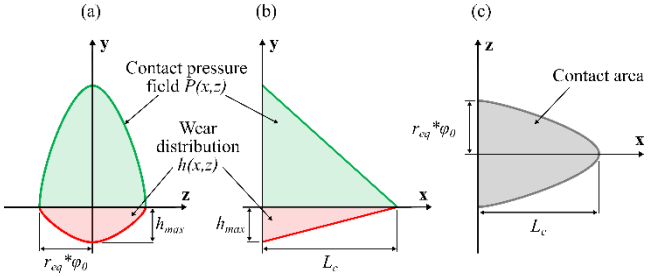


**Fig. 7.** Details of the wear distribution and the contact pressure field between the shaft and the bearings: (a) Plane with normal **x**; (b) Plane with normal **z**; (b) Plane with normal **y**.

The force balance between the bearings and the shaft is made following these assumptions: bodies are supposed rigid and the effects of the clearance and friction are neglected. The contact reaction forces are obtained by solving the force balance in the fixed frame considering the weight of shaft, the weight of the unbalanced mass and the centrifugal force generated by the unbalanced mass fixed at the end of the rotating shaft.

Then, a recursive approach is used to calculate the cumulative wear though time. In each iteration the contact pressure and area, the wear volume, the wear depth and the cumulative wear are computed.

To calculate the contact pressure and area, the contacts are supposed frictionless and under normal pressure only. The following Boussinesq's equation is used:

$$\delta_{max} = \frac{1-\nu}{2\pi G_{eq}} \iint \frac{P(x,z)}{\sqrt{x^2+z^2}}\, dx\, dz \qquad (4)$$

where $\delta_{max}$ is the maximum elastic strain, $\nu$ the Poisson's ratio and $G_{eq}$ equivalent shear modulus. The contact pressure and area are obtained by solving by dichotomy the system of equations. This numerical resolution is used because of the non-linearities of the equations.

The wear volume $\Delta V$ is calculated using the Archard's law:

$$\Delta V = K\, R\, \Delta d \qquad (5)$$

where $K$ is the wear coefficient, $R$ the magnitude of normal reaction force between the shaft and the bearings and $\Delta d$ is the sliding distance.

The wear depth for one revolution is computed from the wear distribution field $h(x,z)$ (represented in red in Fig. 7):

$$h(x,z) = h_{max}\left(1 - \frac{x}{L_c}\right)\cos\left(\frac{\pi\, z}{2 r_{eq}\varphi(x)}\right) \qquad (6)$$

$$\varphi(x) = \pm \sin^{-1}\left(\sqrt{1 - \frac{x}{L_c}}\,\sin(\varphi_0)\right) \qquad (7)$$

where $h_{max}$ is the maximum wear depth, $L_c$ the contact length, $r_{eq}$ the equivalent radius, $\varphi(x)$ the half aperture angle of the contact surface and $\varphi_0$ the maximum half aperture angle. By double integrating Eq. (6) and knowing the wear volume, the maximum wear depth $h_{max}$ can be computed.

To obtain the cumulative wear depth corresponding to each time step $t_i$, the wear depth for one revolution is multiplied by the number of revolutions done during the time step.

Finally, the geometry is updated to take into account the evolution of the contact area and the evolution of the clearance between the shaft and the bearings that increases with wear.

For the stable wear stage, the wear coefficient was supposed constant as done in other works [19,21]. Calibration tests were carried out to determine the wear coefficient according to the operating conditions used in this work. The mean value of the wear coefficients of the calibration tests was then used. The obtained value was equal to 9.955 E-11 mm²/N. By using the calibrated model, the wear depth can be predicted for a given operating condition.

The variability of the input parameters (unbalanced mass, rotational speed, position of the mass, wear coefficient) was taken into account in uncertainty analysis. This was done using the Monte Carlo's method and allowed to derive the confidence intervals of the predicted wear depth. The assumed variations of the input parameters used for Monte Carlo's method are the same as those in [21].

### 2.3. Digital twin fault diagnosis

The aim of the implemented DTs is to detect an unexpected behaviour of the wear in stable stage. An unexpected behaviour is detected when control limits are exceeded. In this work, the fault diagnosis monitors the wear depth and its rate of change. For each DT, the scenarios of detection were identified and explained.

#### 2.3.1. Fault diagnosis rules for data-based DT

For the DT using the data-based model, the wear depth, the mean wear rate and the standard deviation of the wear rate are followed. The wear depth is systematically compared against a fixed threshold. The mean and the standard deviation of the wear rate are compared against the UCL and the LCL defined by the SPC. The DT detects a change of behaviour when at least one of these three parameters exceeds the control limits. In this work, a fault scenario is defined as the excess of one or more control limits.

In order to identify all possible scenarios, a cross-tabulation matrix was build (Table 5). For example, if the wear depth threshold and the control limits of the mean wear rate are exceeded, it corresponds to the scenario D2. A detailed description of these scenarios and the risk of incident that they occur are presented in Table 6. The level of risk that an incident appears is proposed from the authors' appreciation.

| | Wear depth threshold | Limits of the mean wear rate | Limits of the standard deviation of the wear rate | All |
|---|---|---|---|---|
| Wear depth threshold | D1 | D2 | D3 | NA |
| Limits of the mean wear rate | D2 | D4a, D4b | D5a, D5b | NA |
| Limits of the standard deviation of the wear rate | D3 | D5a, D5b | D6 | NA |
| All | NA | NA | NA | D7 |

**Table 5**. Scenarios of detection for the data-based DT.

| | Control limit exceeded | Description | Risk of incident |
|---|---|---|---|
| **D1** | Wear depth threshold | Normal ageing, end of life | *** (2/3) |
| **D2** | - Wear depth threshold<br>- Limits of the mean wear rate | Wear acceleration and end of life | *** (3/3) |
| **D3** | - Wear depth threshold<br>- Limits of the standard deviation of the wear rate | High dispersion of the rate of change and end of life | *** (3/3) |
| **D4a** | Upper limit of the mean wear rate | Wear acceleration | *** (2/3) |
| **D4b** | Lower limit of the mean wear rate | Wear deceleration | *** (1/3) |
| **D5a** | - Upper limit of the mean wear rate<br>- Limits of standard deviation of the wear rate | High dispersion of the wear rate and wear acceleration | *** (2/3) |
| **D5b** | - Lower limit of the mean wear rate<br>- Limits of the standard deviation of the wear rate | Instability and wear deceleration | *** (1/3) |
| **D6** | Limits of the standard deviation of the wear rate | Instability but stable speed | *** (2/3) |
| **D7** | All | Unlikely situation | *** (3/3) |

**Table 6.** Details of scenarios of detection for the data-based DT. The risk of incident is noted from 1 star (low risk) to 3 stars (high risk).

#### 2.3.2. Fault diagnosis rules for physic-based DT

For the DT using the physic-based model, the wear depth and the mean wear rate are monitored. The wear depth is compared against a threshold and to confidence interval. The mean wear rate is compared against to confidence interval too. The confidence intervals were calculated from the numerical model. The DT detects a change of behaviour when at least one of the control limits is exceeded. Possible scenarios are listed in Table 7. A detailed description of these scenarios and the risk of incident that they occur are presented in Table 8.

| | Wear depth threshold | Wear depth confidence interval | Confidence interval of the mean wear rate | All |
|---|---|---|---|---|
| Wear depth threshold | P1 | P2 | P3 | NA |

| | | | | |
|---|---|---|---|---|
| Wear depth confidence interval | P2 | P4a, P4b, P4c | P5 | NA |
| Confidence interval of the mean wear rate | P3 | P5 | P6 | NA |
| All | NA | NA | NA | P7 |

**Table 7.** Scenarios of detection for the physic-based DT.

| | Control limit exceeded | Description | Risk of incident |
|---|---|---|---|
| **P1** | Wear depth threshold | Normal ageing, end of life | *** (2/3) |
| **P2** | - Wear depth threshold<br>- Wear depth confidence interval | Early end of life | *** (3/3) |
| **P3** | - Wear depth threshold<br>- Confidence interval of the mean wear rate | Wear acceleration near the end of life of the system | *** (3/3) |
| **P4a** | Upper limit of the wear depth confidence interval | Higher wear depth than predicted | *** (2/3) |
| **P4b** | Lower limit of the wear depth confidence interval | Lower wear depth than predicted | *** (1/3) |
| **P4c** | Wear depth confidence interval (lower and upper limits) | High dispersion of the wear depth | *** (2/3) |
| **P5** | - Confidence interval of the wear depth<br>- Confidence interval of the mean wear rate | Higher wear depth than predicted and wear acceleration | *** (2/3) |
| **P6** | Confidence interval of the mean wear rate | Wear acceleration | *** (2/3) |
| **P7** | All | Unlikely situation | *** (3/3) |

**Table 8.** Details of scenarios of detection for the physic-based DT. The risk of incident is noted from 1 star (low risk) to 3 stars (high risk).

### 2.3.3. Fault diagnosis test cases

The rules for fault detection described previously were tested in both DT under two situations: normal and abnormal conditions of wear. The aim is to highlight the capacity of the two DTs to detect a change in behaviour that could affect the integrity of the monitored mechanical system.

The normal conditions of wear represent the evolution of the system under the operating conditions described in Section 2.1.1. An unexpected change of behaviour, was designed to obtain the abnormal conditions of wear. In this work, this situation was simulated by altering the wear rate.

In this article, the wear depth threshold was fixed to 10 µm for both models. In abnormal conditions of wear, the wear rate was accelerated by adding 6 µm/h after 6h20 of use to the measured displacement. This acceleration represents an increase loadings of about 3 times the current loads or a deterioration of the contact conditions (i.e. presence of a third body, increase of the wear coefficient).

## 3. Results

### 3.1. Data-based DT

Fig. 8 shows the results of the wear evolution monitoring and the fault diagnosis with the DT using the SPC.

The evolution of the wear under normal conditions is presented in Fig. 8a-c. The mean (Fig. 8b) and the standard deviation (Fig. 8c) of the wear rate stay inside the control limits. The threshold of the wear depth (red line in Fig. 8a) is exceeded after 10h of use. This situation correspond to scenario D1 explained in Section 2.3.1.

The evolution of the wear under abnormal conditions is presented in Fig. 8d-f. The change of behaviour is clearly visible after 6h20 of use in contrast with the normal condition of wear. The control chart of the mean wear rate (Fig. 8e) is the first to detect the fault at about 6h30. This situation corresponds to scenario D4a (Section 2.3.1). Then the threshold of the wear depth (red line in Fig. 8d) is also exceeded at about 7h20. Therefore, at this moment, scenario D4a evolves to scenario D2 (Section 2.3.1). On the control chart of the standard deviation of the wear rate (Fig. 8f), a change of behaviour is visible but not sufficient to exceed the UCL.

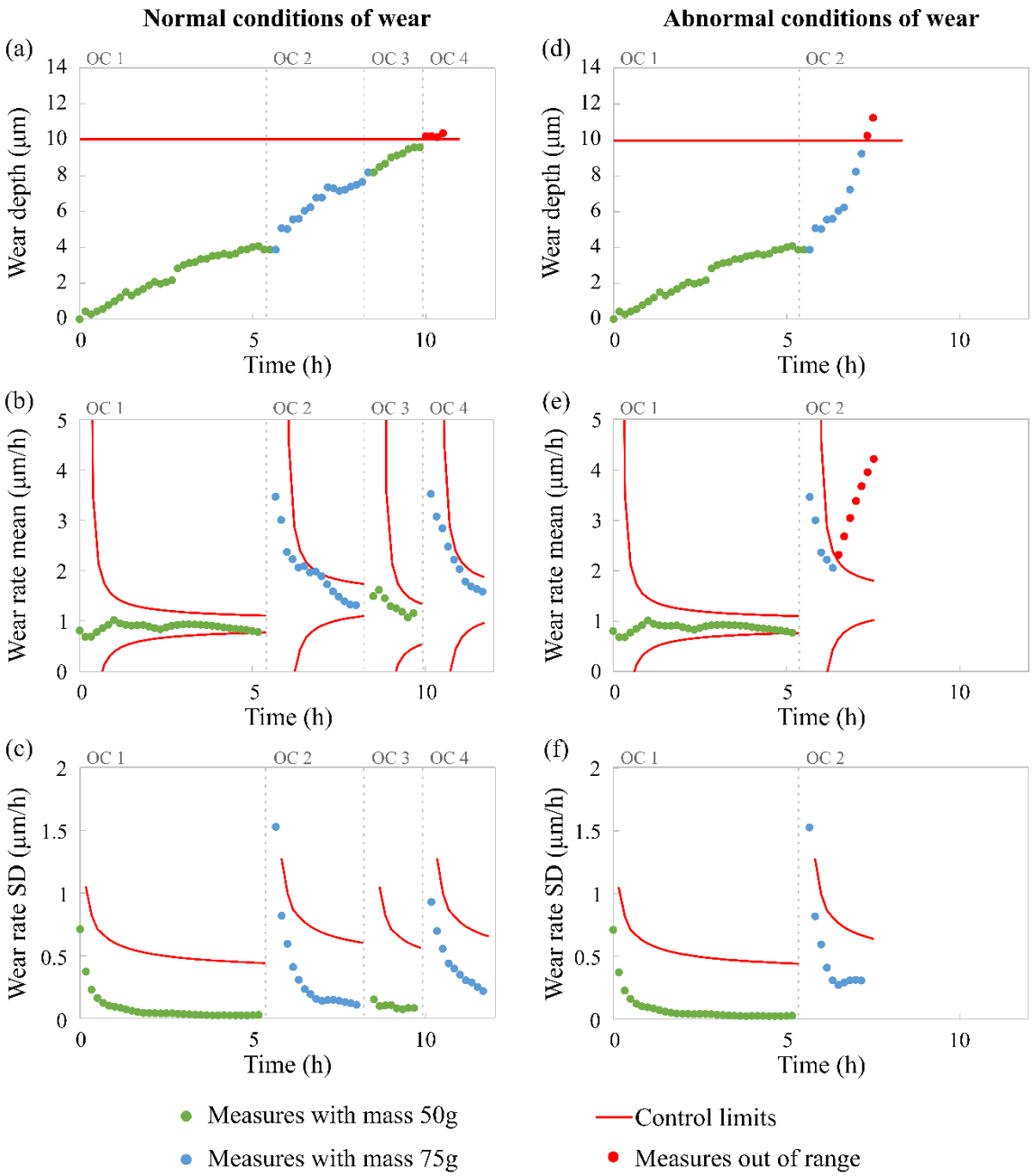


**Fig. 8.** Detection of wear using the data-based DT: left column is the detection in normal use for (a) the wear depth, (b) the mean wear rate and (c) the standard deviation of the wear rate; right column is the detection in abnormal use for (d) the wear depth, (e) the mean wear rate and (f) the standard deviation (SD) of the wear rate. On each graph, the operating conditions (OC) are marked by vertical dotted grey lines.

### 3.2. Physic-based DT

The results of the wear evolution monitoring and the fault diagnosis with the numerical model are presented in Fig. 9.

In normal conditions of wear (Fig. 9a-b), all recorded data stay inside the confidence intervals. The threshold of the wear depth (red line in Fig. 9a) is exceeded after 10h of use. This situation corresponds to scenario P1 explained in Section 2.3.2.

The evolution of the wear under abnormal conditions is presented in Fig. 9c-d. The mean of the wear rate (Fig. 9d) exceeds the control limits at 7h. This situation corresponds to scenario P6 (Section 2.3.2). Then the wear depth (Fig. 9c) exceeds the confidence interval and the threshold simultaneously at about 7h20. At this moment, scenario P6 evolves to scenario P7 (Section 2.3.2).

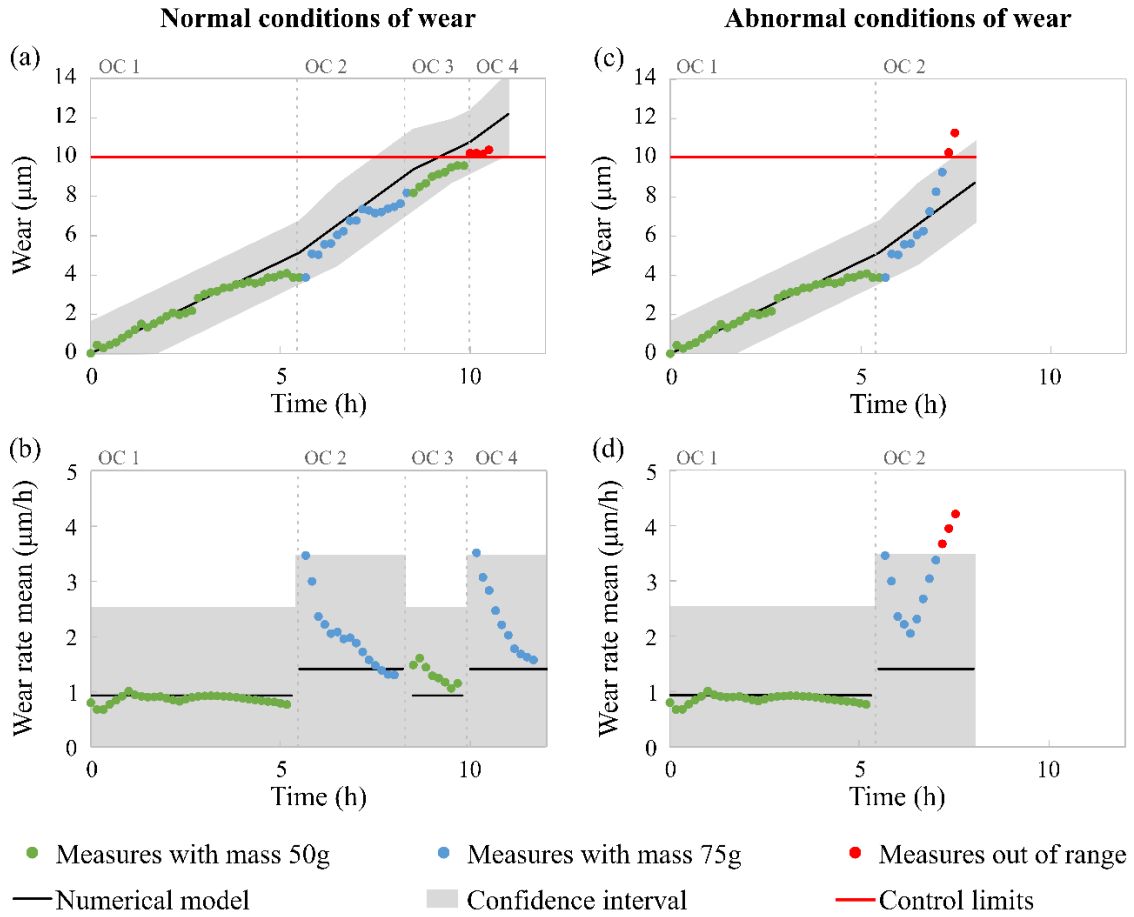


**Fig. 9.** Detection of wear using the physic-based DT: left column is the detection in normal conditions for (a) the wear depth and (b) the mean wear rate; right column is the detection in abnormal conditions for (c) the wear depth and (d) the mean wear rate. On each graph, the operating conditions (OC) are marked by vertical dotted grey lines.

## 4. Discussion

### 4.1. Comparison of detection capacity

Both DTs detect wear in normal and abnormal conditions. The monitoring of the wear rate permits to detect faults earlier than with only the monitoring of the wear depth.

The data-based DT allows to detect faults earlier because the size of the control limits is smaller (except at the very beginning) than those of the numerical model. In order to illustrate that, an overlapping of both control limits for the trial OC 1 (Table 2) is presented in Fig. 10. It can be noticed, that at 5h, $e_2$ is 7 times larger than $e_1$.

The SPC technique is well adapted to the implementation of DT if the target value of the monitored variable is known and if its evolution is linear. If the monitored variable is not linear (i.e. varying speed), the use of higher order statistical tools are necessary. Moreover, to use the SPC a large amount of data is necessary compared to the numerical model.

In this work, the monitored variable can be estimated experimentally, which is not the general case. There exist cases in which only the operating conditions are known. In those cases, the data-based DT cannot be used; in contrast, the physic-based can be, thanks to its predictive capabilities.

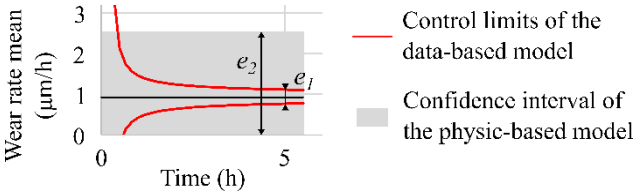


**Fig. 10.** Overlapping of control limits of both DTs implemented.

### 4.2. Comparison with other DTs

In the literature, several DTs of wear based on data analysis or on physical laws were reported. Some of these works are summarized in Table 9. They are compared regarding the cost of implementation and calibration, the computation time, the capability to be re-use and the capability to detect and predict wear. For the comparison, two data-based DTs and two physic-based DTs were analysed. The data-based DTs analysed rely on machine learning [14] and on SPC (as presented in this work). The physic-based DTs analysed rely on FEM [30] and on numerical model (as presented in this work).

From this comparison, it can be concluded that the data-based DTs are easier to implement and execute.

Physic-based DTs are able to detect and predict wear behaviour. If an analytical model is too hard to implement, then a finite elements model is an alternative.

### 4.3. Limitations

The limitations linked to the choices and assumptions to implement the DTs models are discussed in this section.

Only dry contacts were considered in this work to represent the worst operating conditions for a bush bearing system. Indeed, on helicopters, the loss of lubrication leads to run in dry contact conditions that alter the mechanical systems.

In the case studied in this work, the run-out due to clearance is very small regarding the length of the bearings mounted on the frame so the effect of clearance were neglected. About the effects of friction not taken into account, another work [31] shows that friction influences only the location of wear and not the pressure distribution.

To instrument the test bench, the choice was made to use a displacement sensor and a FFT analysis to collect data and nourish the DTs model. Another possibility was to use speed and force sensors to directly have the two input parameters (rotational speed and unbalanced mass) of the DT models implemented.

## 5. Conclusion

In this work, two DTs for monitoring wear were developed and compared. The aim of this work was to demonstrate the proof of concept of DT implemented diagnostic tool for bush bearing wear. The studied physical system is a bush bearing mounted on a test bench. This test bench was instrumented with temperature, acceleration and displacement sensors to monitor wear effects. Both DTs are fed by data recorded on a test bench to monitor the wear depth, the mean wear rate and the standard deviation of the wear rate. To detect wear faults, different scenarios of detection were identified, explained and applied to the two DTs.

The first DT is a data-based model using SPC and the second DT is a physic-based model relying on a numerical model. The two implemented DTs detect abnormal wear but not in the same delay; the data-based allows detects abnormal wear faster. The data-based DT implemented in this work is easier to develop but it is limited to monitoring variable with linear behaviour. If the monitored variable is not linear, the use of higher order statistical tools are necessary (i.e. machine learning). The physic-based DT can predict wear evolution and detect abnormal behaviour by means of confidence intervals. The physic-based DT needs more time to be developed and it is adapted only to contact surfaces defined by analytical geometries.

In future work, the models could be completed to be more realistic by limiting hypotheses taken to implement the model, to predict more variables (temperature, shaft displacement, etc.), to work with more wear cases (running-in, varying of speed, etc.) or even to use more complex input data (vibration signals with harmonics). This work is a contribution for new wear diagnostic tools.


## Acknowledgements

This work was supported by Airbus Helicopters, Aix-Marseille University and ANRT (Association Nationale pour la Recherche et la Technologie) by the grant n° 2019/1242. The experimental devices were founded by: European Community, French Ministry of Research and Education and Aix-Marseille Conurbation Community.


| | **Data-based models** | | **Physic-based models** | |
|---|---|---|---|---|
| | **Machine learning** | **SPC (from this work)** | **FEM** | **Numerical model (from this work)** |
| **Studied case** | Remaining useful lifetime of ball bearing-type contacts [14] | Wear of bearings under dynamic loading | Wear on an oscillatory pin joint [30] | Wear of bearings under dynamic loading [21] |
| **Costs of implementation and calibration** | Training time of about 3 min [14] | Only need target values of the monitored variables | Well adapted for complex geometries, need to calibrate wear coefficient on experimental data [30] | Adapted only for analytical geometries, need to calibrate wear coefficient on experimental data [21] |
| **Computation time** | Not reported | Less than 1 s for 7.8E5 cycles | 3.4 h for 4.1E5 cycles [30] | 22 min for 4.5E6 cycles [21] |
| **Capability to be re-used** | Not reported | Easy to adapt if the target values are known | Need to be the same geometry to avoid re-meshing | Need to be same kind of loadings and geometry |
| **Capability to detect/predict wear** | Good prediction of the remaining useful life (Pearson correlation coefficient = 95.3%) [14] | Early detection of abnormal behaviour | Not reported | Wear prediction and detection of abnormal behaviours |

**Table 9.** Comparison of wear DT models.

## References


[1] J. Kraft, S. Kuntzagk, Engine Fleet-Management: The Use of Digital Twins From a MRO Perspective, in: American Society of Mechanical Engineers, Charlotte, North Carolina, USA, 2017. https://doi.org/10.1115/GT2017-63336.

[2] M. Grieves, Digital Twin: Manufacturing Excellence through Virtual Factory Replication, (2015).

[3] R. Rosen, G. von Wichert, G. Lo, K.D. Bettenhausen, About The Importance of Autonomy and Digital Twins for the Future of Manufacturing, IFAC-Pap. 48 (2015) 567–572. https://doi.org/10.1016/j.ifacol.2015.06.141.

[4] W. Kritzinger, M. Karner, G. Traar, J. Henjes, W. Sihn, Digital Twin in manufacturing: A categorical literature review and classification, IFAC-Pap. 51 (2018) 1016–1022. https://doi.org/10.1016/j.ifacol.2018.08.474.

[5] F. Tao, M. Zhang, Y. Liu, A.Y.C. Nee, Digital twin driven prognostics and health management for complex equipment, CIRP Ann. 67 (2018) 169–172. https://doi.org/10.1016/j.cirp.2018.04.055.

[6] J. Wang, L. Ye, R.X. Gao, C. Li, L. Zhang, Digital Twin for rotating machinery fault diagnosis in smart manufacturing, Int. J. Prod. Res. 57 (2019) 3920–3934. https://doi.org/10.1080/00207543.2018.1552032.

[7] E.J. Tuegel, A.R. Ingraffea, T.G. Eason, S.M. Spottswood, Reengineering Aircraft Structural Life Prediction Using a Digital Twin, Int. J. Aerosp. Eng. 2011 (2011). https://doi.org/10.1155/2011/154798.

[8] R. Söderberg, K. Wärmefjord, J.S. Carlson, L. Lindkvist, Toward a Digital Twin for real-time geometry assurance in individualized production, CIRP Ann. 66 (2017) 137–140. https://doi.org/10.1016/j.cirp.2017.04.038.

[9] F. Tao, M. Zhang, Digital Twin Shop-Floor: A New Shop-Floor Paradigm Towards Smart Manufacturing, IEEE Access. 5 (2017) 20418–20427. https://doi.org/10.1109/ACCESS.2017.2756069.

[10] H. Zhang, Q. Qi, F. Tao, A multi-scale modeling method for digital twin shop-floor, J. Manuf. Syst. 62 (2022) 417–428. https://doi.org/10.1016/j.jmsy.2021.12.011.

[11] P.M. Karve, Y. Guo, B. Kapusuzoglu, S. Mahadevan, M.A. Haile, Digital twin approach for damage-tolerant mission planning under uncertainty, Eng. Fract. Mech. 225 (2020) 106766. https://doi.org/10.1016/j.engfracmech.2019.106766.

[12] S.R. Yeratapally, P.E. Leser, J.D. Hochhalter, W.P. Leser, T.J. Ruggles, A digital twin feasibility study (Part I): Non-deterministic predictions of fatigue life in aluminum alloy 7075-T651 using a microstructure-based multi-scale model, Eng. Fract. Mech. 228 (2020) 106888. https://doi.org/10.1016/j.engfracmech.2020.106888.

[13] L. de C.-E. Kerman, G.-P. Eider, A. Aitor, Towards a Circular Rotating Blade Wear Assessment Digital Twin for Manufacturing Lines, IFAC-Pap. 55 (2022) 561–566. https://doi.org/10.1016/j.ifacol.2022.04.253.

[14] P.S. Desai, V. Granja, C.F. Higgs, Lifetime Prediction Using a Tribology-Aware, Deep Learning-Based Digital Twin of Ball Bearing-Like Tribosystems in Oil and Gas, Processes. 9 (2021) 922. https://doi.org/10.3390/pr9060922.

[15] P.K. Rajesh, N. Manikandan, C.S. Ramshankar, T. Vishwanathan, C. Sathishkumar, Digital Twin of an Automotive Brake Pad for Predictive Maintenance, Procedia Comput. Sci. 165 (2019) 18–24. https://doi.org/10.1016/j.procs.2020.01.061.

[16] Y. Qin, X. Wu, J. Luo, Data-Model Combined Driven Digital Twin of Life-Cycle Rolling Bearing, IEEE Trans. Ind. Inform. 18 (2022) 1530–1540. https://doi.org/10.1109/TII.2021.3089340.

[17] S.L. Chen, L. Wang, R.J.K. Wood, R. Callan, H.E.G. Powrie, Anomaly detection of the tapered roller bearings with statistical data-driven approaches, in: Insight - Non-Destr. Test. Cond. Monit., Stratford-upon-avon, England, 2010: pp. 428–436. https://doi.org/10.1784/insi.2010.52.8.428.

[18] C.H.H. Ratsimba, I.R. McColl, E.J. Williams, S.B. Leen, H.P. Soh, Measurement, analysis and prediction of fretting wear damage in a representative aeroengine spline coupling, Wear. 257 (2004) 1193–1206. https://doi.org/10.1016/j.wear.2004.08.003.

[19] A.A. Schmidt, T. Schmidt, O. Grabherr, D. Bartel, Transient wear simulation based on three-dimensional finite element analysis for a dry running tilted shaft-bushing bearing, Wear. 408–409 (2018) 171–179. https://doi.org/10.1016/j.wear.2018.05.008.

[20] D. Sysaykeo, J.-M. Linares, E. Mermoz, Wear Behavior of a Bio-inspired Bearing for off-center Loads, J. Bionic Eng. 17 (2020) 1251–1262. https://doi.org/10.1007/s42235-020-0107-3.

[21] A. Regis, J.-M. Linares, S. Arroyave-Tobon, E. Mermoz, Numerical model to predict wear of dynamically loaded plain bearings, Wear. 508–509 (2022). https://doi.org/10.1016/j.wear.2022.204467.

[22] P. Flores, Modeling and simulation of wear in revolute clearance joints in multibody systems, Mech. Mach. Theory. 44 (2009) 1211–1222. https://doi.org/10.1016/j.mechmachtheory.2008.08.003.

[23] X. Lai, H. He, Q. Lai, C. Wang, J. Yang, Y. Zhang, H. Fang, S. Liao, Computational prediction and experimental validation of revolute joint clearance wear in the low-velocity planar mechanism, Mech. Syst. Signal Process. 85 (2017) 963–976. https://doi.org/10.1016/j.ymssp.2016.09.027.

[24] S. Akbarzadeh, M.M. Khonsari, Prediction of Steady State Adhesive Wear in Spur Gears Using the EHL Load Sharing Concept, J. Tribol. 131 (2009) 024503. https://doi.org/10.1115/1.3075859.

[25] S.L. Chen, M. Craig, R.J.K. Wood, L. Wang, R. Callan, H.E.G. Powrie, Bearing Condition Monitoring Using Multiple Sensors and Integrated Data Fusion Techniques, (2008) 12.

[26] P. Courrieu, Fast Computation of Moore-Penrose Inverse Matrices, Neural Inf. Process. 8 (2005).

[27] J.-M. Linares, J. Chaves-Jacob, Q. Lopez, J.-M. Sprauel, Fatigue life optimization for 17-4Ph steel produced by selective laser melting, Rapid Prototyp. J. 28 (2022) 1182–1192. https://doi.org/10.1108/RPJ-03-2021-0062.

[28] ISO 8258:1991 - Shewhart control charts, (1991).

[29] R.S. Colbert, L.A. Alvarez, M.A. Hamilton, J.G. Steffens, J.C. Ziegert, D.L. Burris, W.G. Sawyer, Edges, clearances, and wear: Little things that make big differences in bushing friction, Wear. 268 (2010) 41–49. https://doi.org/10.1016/j.wear.2009.06.030.

[30] S. Mukras, N.H. Kim, W.G. Sawyer, D.B. Jackson, L.W. Bergquist, Numerical integration schemes and parallel computation for wear prediction using finite element method, Wear. 266 (2009) 822–831. https://doi.org/10.1016/j.wear.2008.12.016.

[31] L. Mattei, F. Di Puccio, Wear Simulation of Metal-on-Metal Hip Replacements With Frictional Contact, J. Tribol. 135 (2013) 021402. https://doi.org/10.1115/1.4023207.